Self-similar regularization of optic-flow for turbulent motion estimation

Patrick Héas, Etienne Mémin, Dominique Heitz

Self-similar regularization of optic-flow for turbulent motion estimation

Patrick Héas[1,2], Etienne Mémin[1], Dominique Heitz[2]
{Patrick.Heas, Etienne.Memin}@irisa.fr, Dominque.Heitz@cemagref.fr

[1]INRIA, Vista Project, Center of Rennes
[2] CEMAGREF, Center of Rennes

Abstract. Based on self-similar models of turbulence, we propose in this paper a multi-scale regularizer in order to provide a closure to the optic-flow estimation problem. Regularization is achieved by constraining motion increments to behave as a self-similar process. The associate constrained minimization problem results in a collection of first-order optic-flow regularizers acting at the different scales. The problem is optimally solved by taking advantage of lagrangian duality. Furthermore, an advantage of using a dual formulation, is that we also infer the regularization parameters. Since, the self-similar model parameters observed in real cases can deviate from theory, we propose to add in the algorithm a bayesian learning stage. The performance of the resulting optic-flow estimator is evaluated on a particle image sequence of a simulated turbulent flow. The self-similar regularizer is also assessed on a meteorological image sequence.

1 Introduction

The estimation of highly non-rigid image flows is an important problem in various application areas of fluid flow image analysis like remote sensing, medical imaging, and experimental fluid mechanics. Such flows, which cannot be represented by a single parametric model, are typically estimated by variational approaches. In this framework, regularization models are required to remove the motion estimation ambiguities. However, standard regularizers acting in a limited spatial neighborhood are insufficient to recover accurately the multi-scale structures of turbulent flows. Furthermore, they do not rely on any physical prior knowledge and, moreover, raise the open question of tuning the regularizer weight.

The objective of this contribution is to provide a multi-scale regularizer based on turbulent motion self-similarity. In contrast to standard approaches, this self-similar prior is physically sound and presents the valuable advantage of solving the aperture problem while fixing regularizer weights at the different scales. The paper is organized as follows. In the next section, we first highlight the limitation of standard optic-flow regularizers. Besides, we introduce self-similar models issued from theoretical works on turbulence. Then, in section 3, self-similar constraints are defined and a dual approach is proposed to solve optimally constrained optic-flow estimation problems using convex optimization methods. In order to introduce uncertainty in the parameters of the self-similar model given by theory, a bayesian estimation framework is presented in section 4. Finally, a numerical evaluation with synthetic flow and results obtained with experimental data reveal the interest of self-similar regularization for fluid flows.

2 Related work

2.1 Optic-flow state of the art

Aperture problem The apparent motion $\mathbf{v} = (u, v)$, perceived through image intensity $I(\mathbf{s}, t)$ variations, respects the standard Optical Flow Constraint (OFC) observation model:

$$I_t + \mathbf{v} \cdot \nabla I = 0. \tag{1}$$

Apparent motion and the real underlying velocity field are identical when considering rigid motion and stable lighting conditions. For fluids, this identity remains valid in the case of 2D incompressible flows. Based on mass conservation, the integrated continuity equation has been proposed in the literature for various 3D fluid flows visualized in a projected image plane in order to link the image intensity function I to a vertically averaged horizontal velocity field $\mathbf{v}$ [1–3]. However, observation models can not be used alone, as they provide only one equation for two unknowns at each spatio-temporal locations $(\mathbf{s}, t)$. This constitute the so-called aperture problem.

Standard regularizer limitations To deal with this problem, the most common assumption consists in enforcing locally spatial coherence. Global regularization schemes over the entire image domain Ω are convenient to model spatial dependencies on the complete image domain. On the contrary to disjoint estimation approaches [4], dense velocity fields are estimated even in the case of noisy, low contrasted and incomplete observations. More precisely, the motion *a posteriori* estimation problem is defined as the global minimization of an energy function composed of two components:

$$f(I, \mathbf{v}) = f_d(I, \mathbf{v}) + \alpha f_r(\mathbf{v}) \tag{2}$$

The first energy $f_d(\mathbf{v}, I)$, called the data term, penalizes discrepancies from the observation models and thus can be related to a *likelihood* probability. For example, discretizing in time the OFC equation, one can build the data term:

$$f_d(I, \mathbf{v}) = \frac{1}{2} \int_\Omega \phi \left((\tilde{I} - I + \mathbf{v} \cdot \nabla \tilde{I})^2 \right) d\mathbf{s} \tag{3}$$

where $\tilde{I}$ denotes the image $I(t + \Delta t)$. A robust penalty function ϕ can be introduced in the data term for attenuating the effect of observation outliers deviating significantly from the model. In this work, ϕ are *Leclerc* semi-quadratic M-estimator as proposed in [5]. The second component $f_r(\mathbf{v})$, called the regularization term, acts as a spatial *prior* enforcing the solution to follow some smoothness properties. In the previous expression, $\alpha > 0$ denotes a regularization parameter controlling the balance between the smoothness and the global adequacy to the observation model. In this framework, Horn and Schunck [6] proposed a first-order regularization of the two spatial components u and v of velocity field $\mathbf{v}$:

$$f_r(\mathbf{v}) = \frac{1}{2} \int_\Omega ||\nabla u||^2 + ||\nabla v||^2 d\mathbf{s} \tag{4}$$

However, a first order regularization is not adapted to fluid flows as it penalizes spatially non-homogeneous velocity fields. Second order regularizers on motion

vorticity and divergence have been proposed to overcome those limitations [2, 7, 8]. Nevertheless, such regularization models fail to describe the multi-scale structure of turbulent velocity fields. Efficient multi-scale regularizers based on fractal priors have already been introduced in [9]. However, such multi-scale models have not been linked to physical prior on turbulence. Furthermore, using an energy based on two components raises the difficult problem of fixing some regularization parameters.

Multi-resolution approach One major problem with observation models is the estimation of large displacements. Indeed, these equations are only valid if the solution is in the region of linearity of the image intensity function. A standard approach for tackling non-linearity is to apply successive linearizations around a current estimate and to warp a multi-resolution representation of the data accordingly. More precisely, a large displacement field $\tilde{\mathbf{v}}$ is first estimated with the original data term at coarse resolution, where the linearity assumption is valid. Then, introducing the decomposition:

$$\mathbf{v} = \tilde{\mathbf{v}} + \mathbf{v}', \tag{5}$$

motion is refined through an incremental fields $\mathbf{v}'$ estimated using a linearized motion-compensated data term while going down the resolution levels of an image pyramid [10]. Splines are in this context advantageous interpolators useful to derive accurate motion-compensated images at the different resolutions [11].

2.2 Turbulence self-similar models

In the turbulence community, turbulent motion is known to be structured as a scale invariant spatial process. In order to define scale invariance, let us introduce the function of velocitity increments:

$$\delta\mathbf{v}(\mathbf{s}, \boldsymbol{\ell}) = \mathbf{v}(\mathbf{s} + \boldsymbol{\ell}) - \mathbf{v}(\mathbf{s}). \tag{6}$$

where ℓ represents the norm of increment $\boldsymbol{\ell}$. We also introduce the longitudinal $\delta\mathbf{v}_{\parallel}(\ell)$ and transverse $\delta\mathbf{v}_{\perp}(\ell)$ functions defined as $\delta\mathbf{v}_{\parallel}(\mathbf{s}, \ell) = \mathbf{v}(\mathbf{s} + \ell\boldsymbol{t}) - \mathbf{v}(\mathbf{s})$ and $\delta\mathbf{v}_{\perp}(\mathbf{s}, \ell) = \mathbf{v}(\mathbf{s} + \ell\boldsymbol{n}) - \mathbf{v}(\mathbf{s})$, with $\boldsymbol{t}$ and $\boldsymbol{n}$ denoting the tangential and the normal unitary vectors of any bidimensional orthogonal basis of the image plane. No confusion should be made here with the normal and tangential optic-flow components. As a classical hypothesis in turbulence studies, we assume homogeneity and isotropy, that is to say we consider that the statistical properties of the velocity field are invariant under translation of spatial location $\mathbf{s}$ and rotation of $\boldsymbol{\ell}$. In agreement with these assumptions, index to spatial locations $\mathbf{s}$ can be dropped and a simple scalar velocity increment function $\delta v(\ell)$ can be defined in the bidimensional plane either by $\delta\mathbf{v}_{\parallel}(\ell) \cdot \boldsymbol{t}$, $\delta\mathbf{v}_{\parallel}(\ell) \cdot \boldsymbol{n}$, $\delta\mathbf{v}_{\perp}(\ell) \cdot \boldsymbol{t}$ or $\delta\mathbf{v}_{\perp}(\ell) \cdot \boldsymbol{n}$. For any of these scalar quantities, *Kolmogorov* [12] demonstrated that from a statistical point of view the turbulent flow is self-similar, i.e. there exists a unique scaling exponent $h \in \mathbb{R}$ such that:

$$\delta v(\lambda\ell) = \lambda^h \delta v(\ell), \ \ \forall\lambda \in \mathbb{R}^+, \tag{7}$$

A corollary is that the second order moment of the probability distribution function $P_\ell(\delta v)$ of velocity increments, namely the second order structure function:

$$\mathrm{E}[\delta v(\ell)^2] = \int_{\mathbb{R}} \delta v(\ell)^2 P_\ell(\delta v(\ell)) d\delta v(\ell) \tag{8}$$

follows a power law of universal exponent ζ:

$$\mathrm{E}[\delta v(\ell)^2] - \beta \ell^{\zeta} = 0. \tag{9}$$

For three dimensional turbulence, the scale range $\mathbf{I}$ of the power law, so-called *inertial range*, is defined for $\ell \in [\eta, \ell_0]$, where η represents the dissipative scale and where ℓ_0 is much smaller than the diameter L of the largest vortex. In this range, *Kolmogorov* demonstrated that $\zeta = 2/3$. Analogously, for bi-dimensional turbulence with energy injection at scale ℓ_0, *Kraichnan* showed that there exist two different self-similar processes: $\zeta = 2$ within a range $\mathbf{I}_1 = [\eta, \ell_0]$ and $\zeta = 2/3$ within a range $\mathbf{I}_2 = [\ell_0, L]$ [13]. For atmospheric turbulence, measurements proved an inversion of the the two former power laws: $\zeta = 2/3$ within a range $\mathbf{I}_1 = [1, 500]$ kilometers and $\zeta = 2$ within a range $\mathbf{I}_2 = [1000, 3000]$ kilometers [14]. Moreover, for any flow, there exits a power law of scaling exponent $\zeta = 2$ in the dissipative range $\mathbf{I}_0 = [0, \eta]$.

3 Self-similar regularization of optic-flow

In this section we propose to close the optic-flow equations by introducing physical-based self-similar constraints. Besides providing a closure for motion estimation, such a self-similar regularizer yields several benefits:

- first, self-similar processes are multi-scale models which will structure motion fields across scales in agreement with physics,
- second, solving optimally the optic-flow minimization problem under self-similar constraints will lead to a non-parametric method where the problem of fixing regularization parameter α does no longer exist,
- last, the motion estimation problem can be solved using standard convex optimization methods.

3.1 Self-similar constraints

Let us first formalize self-similar constraints. The second order structure function $\mathrm{E}[\delta v(\ell)^2]$ is an expectation defined in Eq. 8. We approximate this expectation by a statistical average over the image domain Ω:

$$\mathrm{E}[\delta v(\ell)^2] \approx \frac{1}{|\Omega|} \int_{\Omega} \delta v(\ell)^2 d\mathbf{s} \tag{10}$$

where $|\Omega|$ denotes the image domain area. In order to obtain an accurate expectation estimator over the bi-dimensional plane and in order to avoid boundary effects, we build a scalar structure function by averaging the norm of transverse and longitudinal structure functions in the 2 directions:

$$\delta v(\ell) = \sqrt{\frac{1}{8}(||\delta \mathbf{v}_{\parallel}(\ell)||^2 + ||\delta \mathbf{v}_{\perp}(\ell)||^2 + ||\delta \mathbf{v}_{\parallel}(-\ell)||^2 + ||\delta \mathbf{v}_{\perp}(-\ell)||^2)} \tag{11}$$

A constraint $g_\ell(\mathbf{v})$ is then defined for each scale ℓ as the difference between the second order structure function depending on the velocity field $\mathbf{v}$, and the predicted power law. Thus, for any scale $\ell \in \cup \mathbf{I}_i$, an estimated motion field should respect the constraint :

$$g_\ell(\mathbf{v}) = \frac{1}{2}(\mathrm{E}[\delta v(\ell)^2] - \beta_i \ell^{\zeta_i}) = 0, \ \forall \ell \in \cup \mathbf{I}_i \tag{12}$$

for given scaling exponent ζ_i and factor β_i.

3.2 Constrained motion estimation problem

Referring to section 2.1, the minimization related to the unclosed optic-flow estimation problem reads:

$$(\hat{\mathbf{v}}) = \arg\min_{\mathbf{v}} f_d(I, \mathbf{v}). \tag{13}$$

Adding the self-similar constraints, we obtain the following constraint minimization problem:

$$\begin{cases} \min_{\mathbf{v}} \ f_d(I, \mathbf{v}) \\ \text{under the constraints:} \\ g_\ell(\mathbf{v}) = 0, \ \ \forall \ell \in \cup \mathbf{I}_i \\ \mathbf{v} \in \mathbb{R}^n \end{cases}. \tag{14}$$

3.3 Discrete problem formulation

Let us now express the constraint problem in its discrete form. The derivatives $\nabla_{\mathbf{v}} f_d(I, \mathbf{v})$ related to any motion-compensated data term (which is quadratic with respect to motion increments $\mathbf{v}'$) can be expressed in the matricial form $A_0\mathbf{v}' - b_0$, when discretized on an image grid $\mathbf{S}$ of m points with a finite difference scheme. The two discretized components of $\mathbf{v}'$ now represents a field of $n = 2m$ variables supported by the grid $\mathbf{S}$, A_0 is a $n \times n$ symmetric positive-definite,$\mathbf{b}_0 \in \mathbb{R}^n$ represents a vector of size n. The discrete data term can be rewritten as:

$$f_d(I, \mathbf{v}) = \frac{1}{2}\mathbf{v}'^T A_0 \mathbf{v}' - \mathbf{b}_0^T \mathbf{v}' + c_0. \tag{15}$$

where $c_0 \in \mathbb{R}$ denotes a scalar. For the self-similar constraints, as detailed in appendix A, the quadratic constraint derivatives can be expressed in the vectorial form $A_\ell \mathbf{v}' - \mathbf{b}_\ell$, where A_ℓ are symmetric positive semi-definite matrices and $\mathbf{b}_\ell$ are vectors of size n. Thus, using discretized variables $\mathbf{v}'$ yields :

$$g_\ell(\mathbf{v}) = \frac{1}{2}\mathbf{v}'^T A_\ell \mathbf{v}' - \mathbf{b}_\ell^T \mathbf{v}' + c_\ell = 0, \ \ \forall \ell \in \cup \mathbf{I}_i, \tag{16}$$

where $c_\ell \in \mathbb{R}$ are scalars. In particular, in appendix A we demonstrate that $A_\ell \mathbf{v}' = \nabla_{\mathbf{v}'} g_\ell(\mathbf{v}')$ and $\mathbf{b}_\ell = -\nabla_{\tilde{\mathbf{v}}} g_\ell(\tilde{\mathbf{v}})$ where the derivative reads:

$$\nabla_{\mathbf{v}} g_\ell(\mathbf{v}) = -\frac{1}{4|\Omega - \{\Gamma_{\boldsymbol{t}}\}|} \begin{pmatrix} \int_{\Omega - \{\Gamma_{\boldsymbol{t}} + \Gamma_{\boldsymbol{n}}\}} \Delta^\ell u \ d\mathbf{s} \\ \int_{\Omega - \{\Gamma_{\boldsymbol{t}} + \Gamma_{\boldsymbol{n}}\}} \Delta^\ell v \ d\mathbf{s} \end{pmatrix} + \text{border terms}, \tag{17}$$

where Δ^ℓ represents a discretized laplacian operators defined on a grid with a mesh equal to ℓ using a centered second order finite difference scheme and where we have exculded vertical $\Gamma_{\boldsymbol{t}}$ and horizontal $\Gamma_{\boldsymbol{n}}$ image borders of width ℓ. The discretized laplacian operators can thus be interpreted as a collection of first-order regularizers performing at the different scales. They represent to some extent a generalization of the *Horn and Schunck* first-order regularizer (Eq. 4) to multi-scale. However, an important difference here is that motion spatial derivatives are not penalized in our case, but constrained to follow a power law across scales.

The constraint motion estimation problem defined in Eq. 14 can thus be rewritten in its discrete form as:

$$(P) \begin{cases} \min_{\mathbf{v}} \ f_d(\mathbf{v}) = \frac{1}{2}\mathbf{v}'^T A_0 \mathbf{v}' - \mathbf{b}_0^T \mathbf{v}' + c_0. \\ \text{under the constraints:} \\ g_\ell(\mathbf{v}) = \frac{1}{2}\mathbf{v}'^T A_\ell \mathbf{v}' - \mathbf{b}_\ell^T \mathbf{v}' + c_\ell = 0, \ \ \forall \ell \in \cup \mathbf{I}_i \\ \mathbf{v} = \mathbf{v}' + \tilde{\mathbf{v}} \in \mathbb{R}^n \end{cases}. \tag{18}$$

where for simplification we have dropped the dependance to the image I.

3.4 Dual problem and optimal solution

A first idea would be to solve P by penalizing with a quadratic cost deviations from the self-similar constraints, i.e. $f(\mathbf{v}) = f_d(\mathbf{v}) + \sum_{\cup \mathbf{I}_i} \alpha_\ell g_\ell(\mathbf{v})^2$, where $\{\alpha_\ell\}$ are positive scalars. Such a multi-scale model would be to some extent similar to the fractal regularizer proposed in [9]. However, this new functional is no longer convex because of $(g_\ell(\mathbf{v}))^2$ and one may face difficulties when resolving non-linear problems and fixing the regularization parameters $\{\alpha_\ell\}$. An advantageous alternative is to solve instead the associated constraint optimization problem using classical lagrangian duality. To define optimality conditions, we now introduce the lagrangian function $L(\mathbf{v}, \boldsymbol{\lambda})$ associated to (P):

$$L(\mathbf{v}, \boldsymbol{\lambda}) = f(\mathbf{v}) + \sum_{\cup \mathbf{I}_i} \lambda_\ell g_\ell(\mathbf{v}), \;\; \boldsymbol{\lambda} = \{\lambda_\ell\}. \tag{19}$$

In the lagrangian duality formalism, the optimal solutions of the so-called *primal* problem P, are obtained by searching *saddle points* of the lagrangian function. *Saddle points* denoted by $(\mathbf{v}^*, \boldsymbol{\lambda}^*)$ are defined as the solutions of the so-called *dual* problem:

$$(D) \left\{ \begin{array}{l} L(\mathbf{v}^*, \boldsymbol{\lambda}^*) = \max_{\boldsymbol{\lambda}} w(\boldsymbol{\lambda}) = \max_{\boldsymbol{\lambda}} \{\min_{\mathbf{v}} L(\mathbf{v}, \boldsymbol{\lambda})\} \\ \lambda_\ell \in \mathbb{R}^+, \;\; \forall \ell \in \cup \mathbf{I}_i \end{array} \right. ,$$

where $w(\boldsymbol{\lambda})$ denotes the *dual* function. As the functions f and g_ℓ are convex and as the constrained group is not empty, for positive and large enough lagrangian multipliers λ_ℓ, L is convex and the minimization problem (P) has a unique *saddle point* i.e. an optimal solution $\mathbf{v}^*$ which is unique[1]. Thus in this framework, each lagrangian multiplier λ_ℓ representing the regularization parameter at scale ℓ can naturally be inferred.

3.5 Convex optimization

The minimum $\hat{\mathbf{v}}'$ of the convex lagrangian function at point $\boldsymbol{\lambda}$ can be obtained by solving the following Euler-Lagrange equations:

$$\nabla_{\mathbf{v}} L(\mathbf{v}, \boldsymbol{\lambda}) = \nabla_{\mathbf{v}} f_d(\mathbf{v}) + \sum_{\cup \mathbf{I}_i} \lambda_\ell \nabla_{\mathbf{v}} g_\ell(\mathbf{v}) = 0. \tag{20}$$

which reduce (using to Eq. 15 and Eq. 16) to solve the linear system :

$$\Big(A_0 + \sum_{\cup \mathbf{I}_i} \lambda_\ell A_\ell\Big) \hat{\mathbf{v}}' = \mathbf{b}_0 + \sum_{\cup \mathbf{I}_i} \lambda_\ell b_\ell. \tag{21}$$

The resolution of Euler-Lagrange large system is efficiently achieved using a conjugate gradient squared optimization method. The dual function is then given by:

$$w(\boldsymbol{\lambda}) = \hat{\mathbf{v}}'^T \Big(A_0 + \sum_{\cup \mathbf{I}_i} \lambda_\ell A_\ell\Big) \hat{\mathbf{v}}' - \Big(\mathbf{b}_0 + \sum_{\cup \mathbf{I}_i} \lambda_\ell b_\ell\Big)^T \hat{\mathbf{v}}' + \mathbf{c}_0 + \sum_{\cup \mathbf{I}_i} \lambda_\ell c_\ell. \tag{22}$$

[1] Let us note that for negative lagrangian multipliers, the convexity of the functional is no longer insured, and for too small lagrangian multipliers, the problem may remain ill-posed with no guarantee of the unicity of the solution. However, in practice the problem admits a solution if there exist at least one scale ℓ with $\lambda_\ell \neq 0$.

The dual function is by definition concave and possesses so-called *sub-gradients* equal to $g_\ell(\hat{\mathbf{v}}' + \tilde{\mathbf{v}})$. We employ a classical gradient method to find $\boldsymbol{\lambda}^*$ which maximizes the dual function and thus obtain the solution $\mathbf{v}^*$. Finally, the constraint motion estimation method results in the *Uzawa* algorithm presented below, which is used to converge towards the unique saddle point $(\mathbf{v}^*, \boldsymbol{\lambda}^*)$, i.e. the optimal motion estimate under self-similar constraints.

- (a) From any initial point $\boldsymbol{\lambda}^0 > 0$ and estimate $\tilde{\mathbf{v}}$:
- (b) At iteration k, find increment $\hat{\mathbf{v}}'$ defining $w(\boldsymbol{\lambda}^k)$ by solving Eq. 21
- (c) Define $\boldsymbol{\lambda}^{k+1}$ by: $\forall \ell \in \cup \mathbf{I}_i,\ \lambda_\ell^{k+1} = \lambda_\ell^k + \rho^k g_\ell(\hat{\mathbf{v}}' + \tilde{\mathbf{v}})$
- (d) If stopping criterion valid :$(\mathbf{v}^*, \boldsymbol{\lambda}^*) = (\hat{\mathbf{v}}' + \tilde{\mathbf{v}}, \boldsymbol{\lambda}^k)$, END.
  Else increment k and go back to (b)

ρ^k denotes the displacement step at iteration k. The latter parameter is adjust at each iteration using a relaxation method proposed in [15].

Uzawa algorithm converging towards $(\mathbf{v}^*, \boldsymbol{\lambda}^*)$**.**

4 Learning turbulence statistics

In this section we consider some uncertainty in the scaling exponent of the self-similar model used for motion estimation. Indeed, there may exist for some particular turbulent flows deviations from theory. The idea is thus to use an *a posteriori* estimation framework to learn the power law parameters based on a coarse motion estimate and theoritical *priors*.

4.1 Prior distribution for scaling exponents

Uncertainty on scaling exponents is introduced in the motion estimation scheme by associating to the unknown self-similar model parameter (ζ, β) an *a priori* Gaussian probability distribution:

$$p(\zeta) \sim \mathcal{N}(\zeta_{K41}, \sigma_\zeta^2) \tag{23}$$

In Eq.23, the mean ζ_{K41} denotes the exponent predicted by Kolmogorov (see section 2.2). We also define a Gaussian likelihood probability distribution at scale ℓ of the logarithm of the structure function:

$$p(\log \mathrm{E}[\delta v(\ell)^2] | \beta, \zeta) \sim \mathcal{N}(log(\beta \ell^\zeta), \sigma^2) \tag{24}$$

Thus, the standard deviation σ_ζ is a parameter tuning the degree of uncertainty on Kolmogorov parameters, while the standard deviation σ represents the allowed deviation of the structure function estimate $\mathrm{E}[\delta v(\ell)^2]$ from the predicted law.

4.2 Learning power laws

Using Eq. 23 and Eq. 24, scaling exponent ζ is estimated using the Maximum *A Posteriori* (MAP) estimator and Bayes law:

$$\hat{\zeta}_{MAP} = \arg\max_{\zeta} p(\zeta) \prod_{\ell \in \mathbf{I}} p(\log \mathrm{E}[\delta v(\ell)^2] | \zeta), \tag{25}$$

where we have assumed that likelihood probabilities $p(\log \mathrm{E}[\delta v(\ell)^2] | \beta, \zeta)$ are independent at the different scale ℓ. In Eq.25, $\mathbf{I}$ denotes a scale interval. As there is usually no *a priori* for β, it is estimated in the sense of the Minimum Mean Square Error (MMSE). Thus, the model parameter $(\hat{\beta}_{MMSE}, \hat{\zeta}_{MAP})$ are obtained by minimization of the functional $J(\beta, \zeta)$:

$$\begin{aligned} (\hat{\beta}_{MMSE}, \hat{\zeta}_{MAP}) &= arg \min_{\beta,\zeta} J(\beta, \zeta) \\ &= arg \min_{\beta,\zeta} \left(\sum_{\ell \in \mathbf{I}} (\log \mathrm{E}[\delta v(\ell)^2] - log(\beta \ell^{\zeta}))^2 + \frac{\sigma^2}{\sigma_{\zeta}^2} (\zeta_{K41} - \zeta)^2 \right) \end{aligned} \tag{26}$$

The minimization is achieved by searching the solution of the linear equations $\nabla_{\beta,\zeta} J(\beta, \zeta) = 0$ based on a coarse estimation of the velocity field with any standard regularizer. Therefore, an analytical solution is obtained by solving the two linear equations.

5 Experiments

To evaluate the performance of the self-similar regularization, a synthetic par-

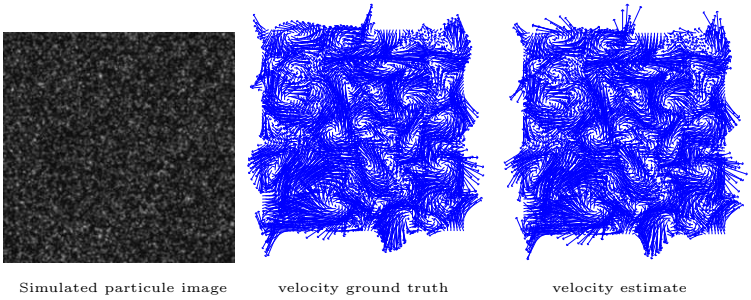

Fig. 1. ***Estimation of two-dimensional turbulence. Left:*** *particle image obtained by DNS of 2D Navier-Stokes equations.* ***Middle:*** *true velocity field* ***Right:*** *estimate*

ticle image sequence was generated based on a two-dimensional turbulent flow obtained by the direct numerical simulation (DNS) of Navier-Stokes equations, and based on a particle image generator [16]. Fig. 1 presents one of the particle images of 256 by 256 pixels, the true underlying velocity field and our estimation obtained by minimizing the OFC based data-term (Eq. 1) under self-similarity constraints. Parameters of the self-similarity model were inferred in the dissipative scale range of $\mathbf{I_0} = [1, 10]$ pixels using a *Horn&Schunck* estimate and a Gaussian prior power exponent centered on the theoretical value of $\zeta_{K41} = 2$ and with standard deviation $\sigma_{\zeta} = 0.3$. Using Eq. 26, we obtained a MAP estimate equal to $\hat{\zeta}_{MAP} = 1.8064$. The estimated power law is plotted in Fig. 2 together with the second order structure function $\mathrm{E}[\delta v(\ell)^2]$ obtained with *Horn&Schunck* algorithm and with the proposed method. Note that constraining motion increments to behave as a self-similar process at small scales yields an enhancement of the structure function at fine but also at large scales. Therefore, one can conclude

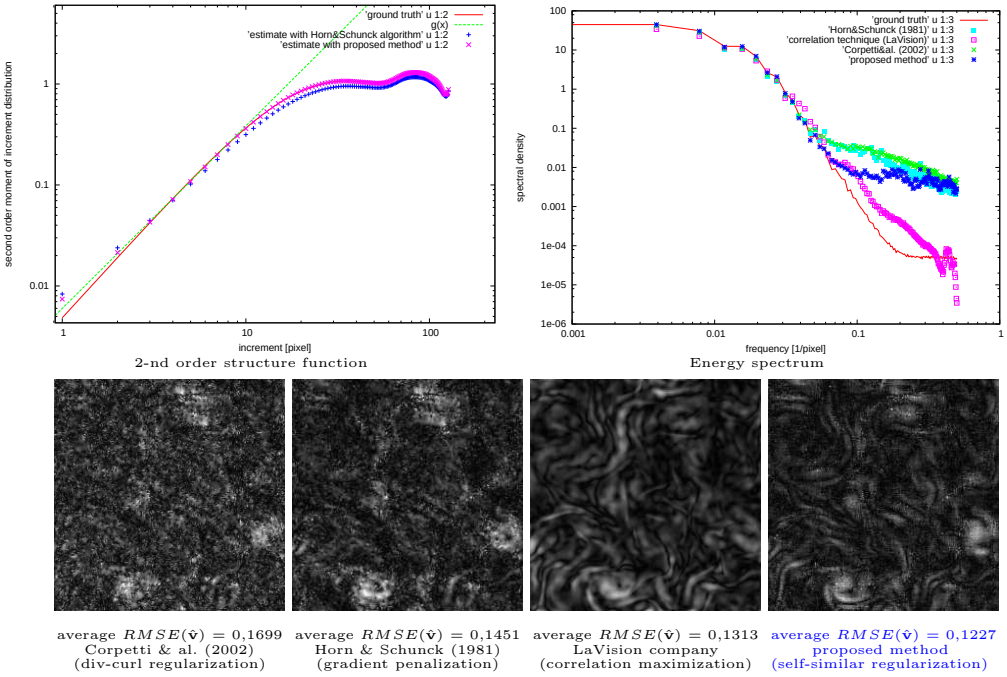

Fig. 2. ***Numerical evaluation of the self-similar regularizer. Upper left:*** *power law $g(x)$ obtained by a posteriori estimation using a Horn&Schunck regularizer. It fits the true and the estimated 2-nd order structure function $E[\delta v(\ell)^2]$ obtained with the proposed regularizer.* ***Upper right:*** *spectral comparison between a first order, a div-curl or a self-similar regularizer and an operational correlation-based method (PIV technique) from LaVision.* ***Below:*** *spatial distribution and average RMSE of different methods.*

that the multi-scale structural information has been propagated through scales. A comparison with the state of the art is also presented in Fig. 2. One can remark that the spatial distribution of the Root Mean Square Errors (RMSE) of velocity field estimated using the self-similar model presents in average much lower values than RMSE obtained with a div-curl [2] or a first order regularizer [6] or even with operational correlation-based techniques. The energy spectrum comparison displayed in the same figure proves that the proposed multi-scale regularization enhances in particular the estimation of small scales displacements. However, large scale enhancements can be also noticed when visualizing energy spectra in natural coordinates.

The multi-scale regularizer has also been assessed on real data. A benchmark has been constituted with a METEOSAT Second Generation meteorological image sequence acquired at a rate of an image every 15 min. The image spatial resolution was $3 \times 3km^2$ at the center of the whole Earth image disk. According to the physical-based methodology presented in [3], sparse image observations related to a layer at intermediate altitude have been derived. Moreover, a robust data term relying on a layer mass conservation model has been used to relate the

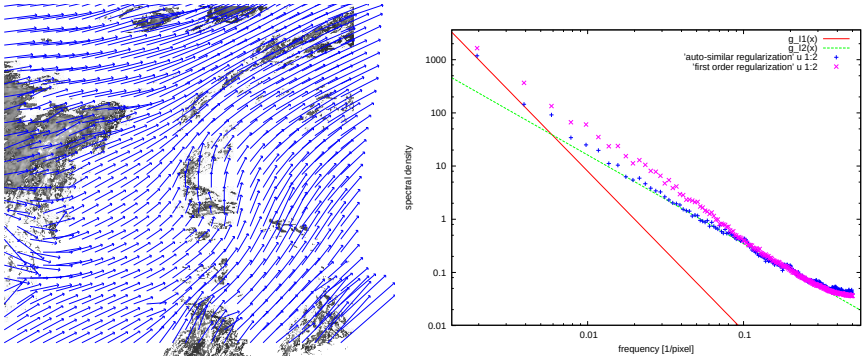

Fig. 3. ***Estimation of atmospheric winds.*** *An horizontal wind field of an atmospheric layer at mid-altitude has been estimated using the physical-based data term proposed in [3] and the self-similar regularizer.* ***Left:*** *estimated velocity field superimposed on a sparse input image of the sequence.* ***Right:*** *estimated energy spectrum fits the power laws* $g_{I_1}(x) \propto x^{-\frac{5}{3}}$ *and* $g_{I_2}(x) \propto x^{-3}$ *known to rule atmospheric flows, on the contrary to results obtained by first order regularization*

image intensity function to a vertically averaged horizontal wind field. Using the predicted power exponents of $\zeta = 2/3$ in a range $\mathbf{I}_1 = [1, 10]$ pixels (contained in the theoretical interval of [1,500] kilometers), parameters $(\hat{\beta}_{MMSE}, \hat{\zeta}_{MAP})$ were derived with Eq. 26 based on a first order regularized solution. Using this learnt power law, the proposed *Uzawa* algorithm was used to converge towards the solution of minimal cost respecting the self-similar constraints. In Fig. 3, one can visualize the estimated velocity field which has been superimposed on a sparse image. A comparison is also provided with a first order regularization in the spectral domain. On the contrary to classical regularization, one can notice that the energy spectrum estimated with the proposed method respects the two power laws known to rule atmospheric flows ($-\zeta - 1 = -5/3$ in $\mathbf{I}_1 = [1, 100]$ pixels and $-\zeta - 1 = -3$ for scales greater than 100 pixels [12, 14]).

6 Conclusions

A closure to the aperture problem for fluid motion estimation is provided in this paper. It relies on constraining motion increments to follow self-similar processes which are well known models in the turbulence community. Solving optimally the associate constrained minimization problem using lagrangian duality leads to a non-parametric method where the problem of fixing regularization parameter does no longer exist. Furthermore, standard convex optimization methods can be used to infer the optimal motion field and its associated lagrangian multipliers. The resulting multi-scale regularizer structures motion fields across scales in agreement with physics. The methods also integrates a learning stage in order to authorize deviations from theory: an *a posteriori* estimation framework is used to infer the power law parameters characterizing the self-similar model. The superiority of the self-similar model on state of the art regularizers is demonstrated on synthetic particle images obtained by simulation of Navier-Stokes equations. Experiments performed on a real meteorological image sequence proves that the

self-similar regularizer enhances the motion spectral-consistency in agreement with atmospheric measurements.

A - Discrete form of the self-similar constraints

From Eq. 10 and Eq. 11, one obtains :

$$\mathrm{E}[\delta v(\ell)^2] \approx \frac{1}{|\Omega|}\int_{\Omega}\frac{1}{8}(||\delta\mathbf{v}_{\parallel}(\ell)||^2+||\delta\mathbf{v}_{\perp}(\ell)||^2+||\delta\mathbf{v}_{\parallel}(-\ell)||^2+||\delta\mathbf{v}_{\perp}(-\ell)||^2)d\mathbf{s} \tag{27}$$

Excluding vertical $\Gamma_{\boldsymbol{t}}$ and horizontal $\Gamma_{\boldsymbol{n}}$ image borders of width ℓ from the calculation of the statistical average, one gets:

$$\begin{aligned}\gamma\mathrm{E}[\delta v(\ell)^2] \approx &\int_{\Omega-\{\Gamma_{\boldsymbol{t}}\}}(||\mathbf{v}(\mathbf{s})-\mathbf{v}(\mathbf{s}+\ell\boldsymbol{t})||^2+||\mathbf{v}(\mathbf{s})-\mathbf{v}(\mathbf{s}-\ell\boldsymbol{t}))||^2)d\mathbf{s} \\ &+\int_{\Omega-\{\Gamma_{\boldsymbol{n}}\}}(||\mathbf{v}(\mathbf{s})-\mathbf{v}(\mathbf{s}+\ell\boldsymbol{n})||^2+||\mathbf{v}(\mathbf{s})-\mathbf{v}(\mathbf{s}-\ell\boldsymbol{n})||^2)d\mathbf{s}\end{aligned} \tag{28}$$

with $\gamma = 8|\Omega-\{\Gamma_{\boldsymbol{t}}\}| = 8|\Omega-\{\Gamma_{\boldsymbol{n}}\}|$. Manipulating the derivate with respect to the motion horizontal component u of the constraints $g_\ell(\mathbf{v})$ which is defined in Eq. 12, one obtains:

$$\begin{aligned}\gamma\nabla_u g_\ell(\mathbf{v}) = &\int_{\Omega-\{\Gamma_{\boldsymbol{t}}\}}(2u(\mathbf{s})-u(\mathbf{s}+\ell\boldsymbol{t})-u(\mathbf{s}-\ell\boldsymbol{t}))d\mathbf{s} \\ &+\int_{\Omega-\{\Gamma_{\boldsymbol{t}}^+\}}(u(\mathbf{s})-u(\mathbf{s}+\ell\boldsymbol{t}))d\mathbf{s}+\int_{\Omega-\{\Gamma_{\boldsymbol{t}}^-\}}(u(\mathbf{s})-u(\mathbf{s}-\ell\boldsymbol{t}))d\mathbf{s} \\ &+\int_{\Omega-\{\Gamma_{\boldsymbol{n}}\}}(2u(\mathbf{s})-u(\mathbf{s}+\ell\boldsymbol{n})-u(\mathbf{s}-\ell\boldsymbol{n}))d\mathbf{s} \\ &+\int_{\Omega-\{\Gamma_{\boldsymbol{n}}^+\)}(u(\mathbf{s})-u(\mathbf{s}+\ell\boldsymbol{n}))d\mathbf{s}+\int_{\Omega-\{\Gamma_{\boldsymbol{n}}^-\}}(u(\mathbf{s})-u(\mathbf{s}-\ell\boldsymbol{n}))d\mathbf{s},\end{aligned} \tag{29}$$

where $(\Gamma_{\boldsymbol{t}}^-,\Gamma_{\boldsymbol{t}}^+)$ and $(\Gamma_{\boldsymbol{n}}^-,\Gamma_{\boldsymbol{n}}^+)$ denote respectively the left and right borders included in $\Gamma_{\boldsymbol{t}}$ and $\Gamma_{\boldsymbol{n}}$. A similar expression can be obtained for the derivate with respect to vertical component v. Noting the presence of laplacian operators in the previous equation, the derivate can thus be rewritten in a compact form:

$$\nabla_{\mathbf{v}} g_\ell(\mathbf{v}) = -\frac{2}{\gamma}\begin{pmatrix}\int_{\Omega-\{\Gamma_{\boldsymbol{t}}+\Gamma_{\boldsymbol{n}}\}}\Delta^\ell u\ d\mathbf{s}\\ \int_{\Omega-\{\Gamma_{\boldsymbol{t}}+\Gamma_{\boldsymbol{n}}\}}\Delta^\ell v\ d\mathbf{s}\end{pmatrix} + \text{border terms}, \tag{30}$$

where Δ^ℓ represents a two-dimensional discretized laplacian operators defined on a grid with a mesh equal to ℓ using a centered second order finite difference scheme. Considering now the velocity field decomposition $\mathbf{v} = \tilde{\mathbf{v}} + \mathbf{v}'$ used in multi-resolution, as the operator is linear one obtains:

$$\nabla_{\mathbf{v}} g_\ell(\mathbf{v}) \ = \nabla_{\tilde{\mathbf{v}}} g_\ell(\tilde{\mathbf{v}}) + \nabla_{\mathbf{v}'} g_\ell(\mathbf{v}') \tag{31}$$

Using Eq. 29 and discretizing the velocity field, the constraints can finally be written in their discrete form:

$$g_\ell(\mathbf{v}) = \frac{1}{2}\mathbf{v}'^T A_\ell \mathbf{v}' - \mathbf{b}_\ell^T \mathbf{v}' + c_\ell = 0 \tag{32}$$

where $A_\ell \mathbf{v}' = \nabla_{\mathbf{v}'} g_\ell(\mathbf{v}')$, $\mathbf{b}_\ell = -\nabla_{\tilde{\mathbf{v}}} g_\ell(\tilde{\mathbf{v}})$ and

$$c_\ell = -\frac{\beta \ell^\zeta}{2} + \frac{1}{2\gamma} \sum_{\Omega - \{\Gamma_{\boldsymbol{t}}\}} ||\tilde{\mathbf{v}}(\mathbf{s}) - \tilde{\mathbf{v}}(\mathbf{s} + \ell \boldsymbol{t})||^2 + ||\tilde{\mathbf{v}}(\mathbf{s}) - \tilde{\mathbf{v}}(\mathbf{s} - \ell \boldsymbol{t}))||^2 d\mathbf{s}$$
$$+ \frac{1}{2\gamma} \sum_{\Omega - \{\Gamma_{\boldsymbol{n}}\}} ||\tilde{\mathbf{v}}(\mathbf{s}) - \tilde{\mathbf{v}}(\mathbf{s} + \ell \boldsymbol{n})||^2 + ||\tilde{\mathbf{v}}(\mathbf{s}) - \tilde{\mathbf{v}}(\mathbf{s} - \ell \boldsymbol{n})||^2 d\mathbf{s}$$

References

1. Fitzpatrick, J.: The existence of geometrical density-image transformations corresponding to object motion. Comput. Vision, Graphics, Image Proc. **44** (1988) 155–174
2. Corpetti, T., Mémin, E., Pérez, P.: Dense estimation of fluid flows. IEEE Trans. Pattern Anal. Mach. Intell. **24** (2002) 365–380
3. Heas, P., Memin, E., Papadakis, N., Szantai, A.: Layered estimation of atmospheric mesoscale dynamics from satellite imagery. IEEE trans. on Geo. and Rem. Sensing **45** (2007) 4087–4104
4. Lucas, B., Kanade, T.: An iterative image registration technique with an application to stereovision. In: Int. Joint Conf. on Artificial Intel. (IJCAI). (1981) 674–679
5. Black, M., Anandan, P.: The robust estimation of multiple motions: Parametric and piecewise-smooth flow fields. Computer Vision and Image Understanding **63** (1996) 75–104
6. Horn, B., Schunck, B.: Determining optical flow. Artificial Intelligence **17** (1981) 185–203
7. Suter, D.: Motion estimation and vector splines. In: Proc. Conf. Comp. Vision Pattern Rec., Seattle, USA (1994) 939–942
8. Yuan, J., Schnoerr, C., Memin, E.: Discrete orthogonal decomposition and variational fluid flow estimation. Journ. of Math. Imaging & Vison **28** (2007) 67–80
9. Luettgen, M., Karl, W., Willsky, A.: Efficient multiscale regularization with applications to the computation of optical flow. IEEE Trans. Im. Processing **3** (1994) 41–64
10. Bergen, J., Burt, P., Hingorani, R., Peleg, S.: A 3-frame algorithm for estimating two-component image motion. IEEE Trans. Pattern Anal. Mach. Intell. **14** (1992) 886–895
11. Unser, M.: Splines: A perfect fit for signal and image processing. IEEE Signal Processing Magazine **16** (1999) 22–38
12. Frisch, U.: Turbulence : the legacy of A.N. Kolmogorov. Cambridge university press (1995)
13. Kraichnan, R.: Inertial ranges in two-dimensional turbulence. Phys. Fluids **10** (1967) 1417–1423
14. Lindborg, E.: Can the atmospheric kinetic energy spectrum be explained by two-dimensional turbulence. J. Fluid Mech. **388** (1999) 259–288
15. Minoux, M.: Programmation mathématique : théorie et algorithmes. Dunod Editions (1983)
16. Carlier, J., Wieneke, B.: Report 1 on production and diffusion of fluid mechanics images and data. Fluid project deliverable 1.2. http://www.fluid.irisa.fr (2005)